Applied Catalysis B: Environmental 160–161 (2014) 325–334

Contents lists available at ScienceDirect

Applied Catalysis B: Environmental

journal homepage: www.elsevier.com/locate/apcatb

Rapid degradation of sulfonamides in a novel heterogeneous sonophotochemical magnetite-catalyzed Fenton-like (US/UV/Fe_3O_4/oxalate) system

Tao Zhou[a,*], Xiaohui Wu[a], Juan Mao[a], Yanrong Zhang[a], Teik-Thye Lim[b,c,**]

[a] School of Environmental Science and Engineering, Huazhong University of Science and Technology, Wuhan 430074, PR China
[b] School of Civil and Environmental Engineering, Nanyang Technological University, 50 Nanyang Avenue, Singapore 639798, Singapore
[c] Nanyang Environment & Water Research Institute (NEWRI), Nanyang Technological University, 1 Cleantech Loop, CleanTech One, Singapore 637141, Singapore

ARTICLE INFO

Article history:
Received 3 January 2014
Received in revised form 2 May 2014
Accepted 20 May 2014
Available online 29 May 2014

Keywords:
Sonophotochemistry
Fenton-like
Sulfonamides
Iron–oxalate
Magnetite

ABSTRACT

A novel sonophotochemical Fenton-like system was investigated in this study for degradation of antibiotic sulfamethazine (SMZ). In the presence of oxalic acid (Ox), the heterogeneous Fe_3O_4-catalyzed system (US/UV/Fe_3O_4/Ox) could induce in-situ generation of H_2O_2 and also Fenton-like reaction. A Significant synergistic SMZ degradation including significantly enhanced SMZ mineralization and detoxification was achieved in the system, as compared to its corresponding individual systems. Ultrasound (US) treatment could eliminate the initial lag period of SMZ degradation which appeared in UV/Fe_3O_4/Ox system without the pre-dissolution phase. This phenomenon was evidenced by significant enhancements in the initial dissolution rate of the iron oxides as well as production rate of the reactive oxygen species (ROS). A reaction mechanism involving a heterogeneous/homogenous iron cycle and a series of homogenous radical reactions was proposed. The promotional role of US could be mostly ascribed to the sonochemcial cavitation effect in both heterogeneous solid–liquid interphase reactions and homogenous radical reactions. The cleavage of S—N bond via •OH attack would be the main SMZ decomposition pathway. The solution pH and [Fe_3O_4:Ox] ratio were the two important factors for SMZ degradation. The repeating SMZ degradation tests of the US/UV/Fe_3O_4/Ox system also suggested that Fe_3O_4 was a favorable catalyst for application of the system in wastewater treatment.

1. Introduction

In the past decade, pharmaceuticals and personal care products (PPCPs) have been becoming a class of contaminants of emerging concern and most of which have been already listed by US EPA as pseudo-persistent pollutants. As a typical class of antibiotics and PPCPs, sulfonamides are widely used in human and veterinary medicine as antibacterial drugs and growth promoters [1]. The appearances of sulfonamides and their metabolites in the aquatic environment raise concerns of their potential adverse effects on human health and the aquatic ecosystem [1–4].

Advanced oxidation processes (AOPs) were successfully used in the past decades as effective alternatives for degrading many toxic and biorefractory organic pollutants which are resistant to the conventional biological treatment technologies [5]. Fenton reaction (or Fenton process) is one of the most commonly used AOPs for environmental applications. With the formation of highly reactive and non-selective hydroxyl radical (•OH) yielded by ferrous iron interaction with hydrogen peroxide, the traditional Fenton reagent has been well established as effective for destruction of organic pharmaceuticals [5]. However, the rapid consumption but very slow regeneration of ferrous, as well as the usage of unstable and self •OH-scavenging H_2O_2 have been the great challenges for the practical applications [6].

In the early 1990s, Zuo and Hoigne [7,8] reported the in-situ generation of reactive oxygen species (ROS) as a result of the solar photolysis of Fe(III)-oxalate complexes in atmospheric

* Corresponding author at: School of Civil and Environmental Engineering, Nanyang Technological University, 50 Nanyang Avenue, Singapore 639798, Republic of Singapore. Tel.: +65 67906933; fax: +65 67910676.
** Corresponding author at: School of Environmental Science and Engineering, Huazhong University of Science and Technology, Wuhan 430074, PR China. Tel.: +86 27 87792101; fax: +86 27 87792101.
E-mail addresses: zhoutao@hust.edu.cn (T. Zhou), cttlim@ntu.edu.sg (T.-T. Lim).

http://dx.doi.org/10.1016/j.apcatb.2014.05.036
0926-3373/

water. Thereafter, the photochemical characteristics of iron species/oxalate systems have received many investigations, since these systems could initiate homogeneous or heterogeneous photo-Fenton-like reactions which could be more effective than the traditional Fenton system in degrading organic contaminants [9–14]. The redox cycling of iron could occur rapidly in the light-irradiated Fe(III)/oxalate systems [13–15] due to the much faster photochemical generation rate of Fe(II) and ca. 3–4 orders of magnitude of •OH yield rate from the reaction of H_2O_2 with Fe(II)-oxalate complexes than with free ferrous ions [16,17].

As compared to the homogenous photochemical Fe(III)/oxalate systems, heterogeneous photochemical Fe(III)/oxalate systems should be more viable for industrial application, because the naturally-occurring Fe(III) oxides are omnipresent and susceptible to light excitation [18]. It was reported that these heterogeneous photochemical systems could efficiently degrade many harmful organic pollutants such as diuron, pentachlorophenol, bisphenol A and azo dyes [6,12,14,18–21]. In such systems, several Fe(III) oxides have been investigated, including goethite (α-FeOOH), hematite (α-Fe_2O_3), maghemite (γ-Fe_2O_3), lepidocrocite (γ-FeOOH), schwertmannite ($Fe_{16}O_{16}(OH)_y(SO_4)_z{\cdot}nH_2O$) and iron corrosion products. Nevertheless, there was obvious discrepancy in the degradation efficiencies of the organics with different kinds of iron oxides. It was mainly because the interfacial reactions on the iron oxides surface are the rate-determining step of all reactions in the photochemical iron oxides–oxalate systems [14,17,18]. The iron oxides with different crystal structures and surface characteristics could affect strongly the rates of ROS production and degradation of target organic pollutants in the systems.

Ultrasound (US) technology is an effective physiochemical method to increase the reaction efficiency of common AOPs. Katsumata et al. [22] and Zhou et al. [23] reported that the significant synergistic degradation and mineralization of fenitrothion and reactive *black* 5 could be achieved in the homogeneous US/UV/Fe(III)–oxalate systems. Considering that the combined sonochemical and mechanical effects could occur in either solid–liquid interphases or bulk solutions [24,25], it is believed that US could significantly improve the efficiency of the heterogeneous photochemical iron oxides–oxalate system. In addition, due to its Fe(II) component, Fe_3O_4 could be also efficient in catalyzing a heterogeneous sonochemical Fenton-like reaction system (US/Fe_3O_4/H_2O_2).

Fe_3O_4 is the only abundant natural iron oxide with Fe^{II} content and has gained a considerable attention over other iron oxides due to its unique characteristics [26]. With a spinel structure and Fe^{II} in the octahedral position, Fe_3O_4 can be easily separated from its reaction systems by magnetic methods. Fe_3O_4 also dissolves faster in solution than other iron oxides and accordingly, it has a higher electron mobility in its spinel structure [27]. However, to our best knowledge, investigation on Fe_3O_4-catalyzed heterogeneous photochemical Fe-oxalate systems for pollutant elimination has been scarcely reported. Furthermore, US could be expected to improve the efficiency of the heterogeneous Fe_3O_4-catalyzed systems, while the reaction mechanism and the role of US still remain uncertain.

Therefore, in this study, a novel heterogeneous sonophotochemical Fe_3O_4/oxalate system (US/UV/Fe_3O_4/Ox) was investigated for the degradation of a sulfonamide, sulfamethazine (SMZ). The objectives of the study were to: (a) examine the synergistic degradation of SMZ achieved in the US/UV/Fe_3O_4/Ox system, (b) evaluate the role of the pre-dissolution phase in three comparable systems (i.e., UV/Fe_3O_4/Ox, US/UV/Fe_3O_4/Ox and US/UV/goethite(α-FeOOH)/Ox systems), (c) reveal the reaction mechanism and promotional role of US in the US/UV/Fe_3O_4/Ox system, (d) explore possible pathways during SMZ degradation, and (e) investigate the effects of several important operating factors and repeating tests on the degradation of SMZ.

2. Materials and methods

2.1. Chemicals

Purified (>99%) sulfamethazine, powder magnetite (Fe_3O_4, >95%, particle size <5 μm) and goethite (α-FeOOH, ~35% Fe) were obtained from Singapore Sigma-Aldrich Company, respectively. Pure oxalic acid (Ox) was supplied by Singapore Merck. Other commonly used chemicals such as $Fe(NO_3)_3$, NaOH, $HClO_4$, $NaClO_4$ and the reagents for sample analysis, were all purchased from Singapore Sigma-Aldrich. Deionized water with resistivity of 18.2 MΩ cm (Millipore Co.) was used for solution preparation throughout the study.

2.2. Experiments

A 600 mL jacket glass reactor equipped with a 9 W UVA lamp (NEC FL8 BL-B, λ_{max} = 365 nm) and an US probe (Misonix) was used in this study. The solution temperature in the reactor was automatic kept at 20 ± 1 °C through a cooling water circulator. The intensity of UVA irradiation was measured as 7.7 ± 0.1 mW cm^{-2} (VECTOR H410 radiometer, Scientech Boulder CO., USA). Continuous ultrasonic shockwave was generated by a sonicator with 20 kHz frequency (XL2020, Misonix Incorporated, New York, USA). Purified air was supplied into the reactor via a glass diffuser at 1.0 L min^{-1} of flowrate and the solution was intensively magnetic-mixed (700 rpm).

Unless otherwise stated, the experimental runs were started with the addition of certain amounts of magnetite particles into aqueous solutions containing the desired initial concentrations of SMZ and oxalic acid. The reaction was immediately commenced by switching on the lamp and sonicator simultaneously. Before the reaction, initial pH was adjusted by using 0.1 M $HClO_4$ or NaOH. In several cases, pre-dissolution of the magnetite particles in the presence of oxalic acid chelation was conducted in dark for 30 min prior to the sonophotochemical or photochemical reactions. During the experiments, samples were withdrawn at specific time intervals and analyzed immediately after filtration through 0.45 μm membrane.

2.3. Analysis

The concentrations of SMZ and oxalate were analyzed by HPLC (WATERS 2695) equipped with a XTerra C18 column and a photodiode array detector (WATERS 2996). With respect to the analysis of SMZ and oxalic acid, the HPLC mobile phase was a mixture of methanol and MQ water (V/V = 40%:60%) and a mixture of 20 mmol KH_2PO_4 buffer (pH = 2.2) and acetonitrile (V/V = 95%:5%), respectively. The flow rate and the determined wavelength were set at 0.5 mL min^{-1} and 1 mL min^{-1}, 260 nm and 220 nm correspondingly.

The mineralization degree of samples was determined by a Shimadzu TOC analyzer (TOC-500, Singapore). The acute ecotoxicity (EC_{50}) of samples was evaluated by a method of luminescent marine bacteria *Vibrio fischeri* measurement (SDI® Microtox 500 Analyzer, USA). The detailed procedure has been described elsewhere [23].

Released inorganic anions (such as sulfate, nitrate and nitrite) during the reaction process were analyzed with a Dionex ICS-1000 ion chromatography (IC) system equipped with an IonPac AS15 anion-exchange column (4 × 250 mm) and a conductivity detector. A mobile phase of 36 mM KOH at a flow rate of 1.2 mL min^{-1} was

adopted. The production of NH_4^+ was identified by using the colorimetric nesslerization method (HACH Method 8038) with a HACH DR/2400 spectrophotometer.

The organic intermediates were examined with a gas chromatograph (Agilent 6890, USA) equipped with a 30 m × 0.25 μm HP5 column and mass selective detector. The column temperature was programmed from 60 °C (held for 2 min) to 285 °C (held for 2 min) at a rate of 10 °C min^{-1}. MS was operated in electron ionization mode (70 eV) and the spectra were obtained at a scan range from m/z 33–500 with a scan time of 0.3 s and interscan of 0.01 s. Before the analysis, 250 mL selected sample was concentrated and extracted by using HLB C18 columns (Waters Oasis®).

A DPD (*N*,*N*-diethyl-*p*-phenylendiamine) spectrophotometrical method [28] was used to measure the concentration of generated H_2O_2. And a dimethyl sulfoxide (DMSO) trapping method was adopted to determine the accumulated •OH concentration throughout the reaction [29]. In this method, indirectly quantified of •OH concentration is determined, through the HPLC examination of a indicative compound (DNPH–HCHO) formed by the reaction between 2,4-dinitrophenyl-hydrazine (DNPH) and the •OH-DMSO adduct.

The concentration of dissolved ferrous species was measured by the *o*-phenanthroline colorimetric method (λ = 510 nm, $\varepsilon = 1.1 \times 10^4\ M^{-1}\ cm^{-1}$). An inductively coupled plasma–optical emission spectrometry (ICP–OES, Optima 2000DV, PerkinElmer Instruments) was used to determine the total dissolve iron species in water samples. The concentrations of the dissolved ferric species could be thus concluded as the subtraction values of $C_{\text{Total dissolved Fe}}$ to $C_{Fe^{(II)}}$.

The solid surface of the fresh and reacted magnetite was analyzed using JEOL JSM6360 scanning electron microscope (SEM). X-ray diffraction (XRD) patterns of the corresponding solids samples were further characterized by a Bruker D8 ADVANCE X-ray Diffractometer with Cu $K\alpha$ radiation (λ = 1.5418 Å) in a 2θ range of 5–80°. Before the characterization procedures, the solids were taken from the reactor, washed by degassed deionized water, and then freeze-dried in vacuum overnight.

3. Results and discussions

3.1. Synergistic SMZ degradation in the heterogeneous US/UV/Fe_3O_4/Ox system

Seven different combined systems of US, UV, Fe_3O_4 and oxalate were investigated for the degradation of SMZ. From Fig. 1a, it can be seen that marginal degradation of SMZ was obtained in either US/UV/Ox system or UV/Fe_3O_4 system, indicating that the SMZ molecule is difficult to be decomposed by photolysis or sonication. Slow SMZ degradations (ca. 10–20% after 60 min of reaction time) were also observed in the US/Fe_3O_4, US/UV/Fe_3O_4 and US/Fe_3O_4/Ox systems, whereas faster degradation of SMZ was achieved in the UV/Fe_3O_4/Ox system. It implied the more production of ROS was achieved in the latter (photochemical complexion system) than the former (US/Fenton-like systems). More rapid degradation of SMZ was found in the US/UV/Fe_3O_4/Ox system, demonstrating the significant synergy achieved in the combined heterogeneous sonophotolytic system compared to the above six systems. It was found that the SMZ degradation process in US/UV/Fe_3O_4/Ox system could be well described by the pseudo-first order kinetic with a k_{obs} of $3.5 \pm 0.2 \times 10^{-2}\ min^{-1}$ ($R^2 = 0.983$). The value is about 10 times larger than that obtained in the US/Fe_3O_4/Ox system ($k_{obs} = 0.36 \pm 0.06 \times 10^{-2}\ min^{-1}$). However, the degradation of SMZ in the UV/Fe_3O_4/Ox system could not follow the pseudo-first order kinetic, because there was an initial degradation lag period. This interesting phenomenon has been scarcely considered in the previous studies where pre-adsorption/dissolution of the added iron oxides with oxalic acid chelation were generally carried out before the commence of degradation reactions [14,17,18,20,21]. The related explanation will be further described in Section 3.3.

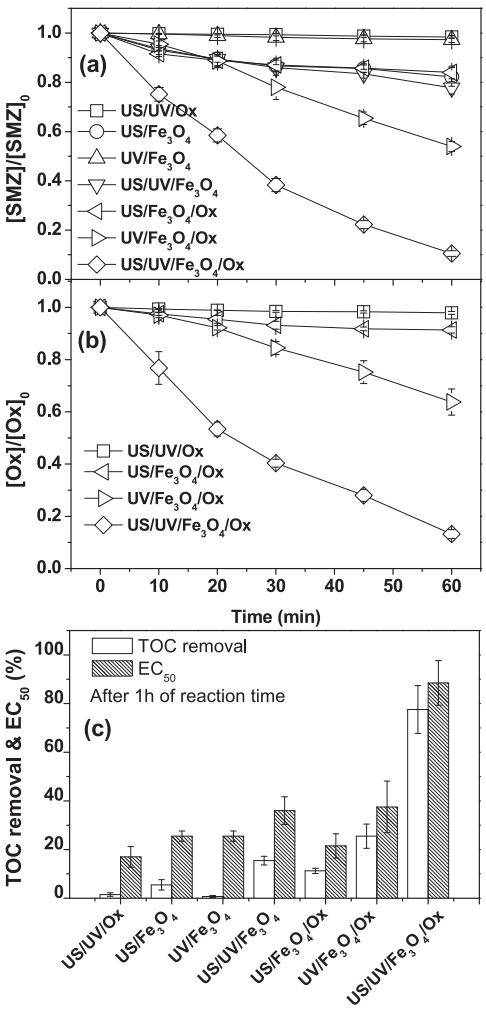

Fig. 1. Degradation efficiencies in the different systems versus the reaction time (a) SMZ degradation; (b) oxalic acid decomposition, (c) TOC removal and acute toxicity EC_{50}. (Initial parameters: 25 mg L^{-1} SMZ, 0.4 g L^{-1} Fe_3O_4, 0.8 mM oxalic acid, 330 W US input power and initial pH 3). Error bars represent 95% confidence limits.

Oxalic acid could be also degraded simultaneously with the SMZ elimination. Among the four systems containing oxalic acid, the role of oxalic acid would be different during the SMZ degradation. In the US/UV/Ox and US/Fe_3O_4/Ox systems, oxalate would mostly play the role as a competitive pollutant. However, oxalic acid would play multiple roles in the UV/Fe_3O_4/Ox and US/UV/Fe_3O_4/Ox systems, as a pollutant and a ROS initiator. As shown in Fig. 1b, the degradation time course of oxalic followed similar trend that of SMZ. The value of the corresponding k_{obs} (oxalate) is $3.2 \pm 0.2 \times 10^{-2}\ min^{-1}$ ($R^2 = 0.985$) in the US/UV/Fe_3O_4/Ox system.

The significant synergistic degradation of SMZ could be further evidenced by the results of mineralization and detoxification of the treated water samples. As depicted by Fig. 1c, 78% of TOC was removed in the US/UV/Fe_3O_4/Ox system after 1 h of reaction time, with increase of the corresponding EC_{50} from 17% (the raw sample) to 89%. The efficiencies of mineralization and detoxification were much higher than those achieved in the other six systems, indicating the significant synergistic degradation of SMZ in the US-irradiated Fe_3O_4/Ox systems.

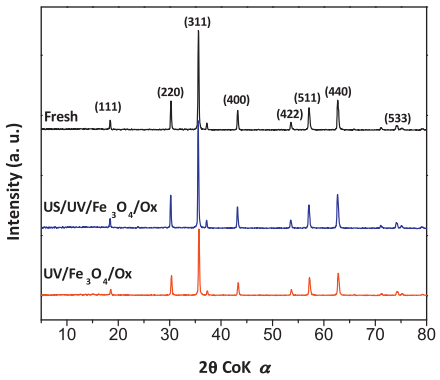

Fig. 2. XRD patterns of the fresh Fe_3O_4 and reacted Fe_3O_4 samples (1 h of usage).

3.2. Surface characteristics of the fresh and reacted Fe_3O_4 particles

The surface characteristics of the fresh and reacted (after 1 h of reaction) Fe_3O_4 samples were examined with XRD and SEM. As shown in Fig. 2, the XRD pattern of the fresh sample depicts that the Fe_3O_4 particles used in this study was of good crystalline, due to its similar XRD pattern to that reported in the XRD standard data base library [27]. It was noted that almost all peaks of the Fe_3O_4 remained after 1 h of reaction time in either the US/UV/Fe_3O_4/Ox system or the UV/Fe_3O_4/Ox system, whereby the peaks area of the latter was smaller. This implied that the surface of Fe_3O_4 could be continuously regenerate under US irradiation, while the reacted Fe_3O_4 surface in the UV/Fe_3O_4/Ox system would be gradually covered by some amorphous iron hydroxides [30].

Fig. 3 presents the SEM morphologies of the fresh Fe_3O_4 and the reacted Fe_3O_4 particles in different systems. From the figure, it can be seen that the Fe_3O_4 particles has been rigorously cleaned after 1 h of US irradiation (Fig. 3a and b). It implied that not only the BET surface area but also the pore size and volume of the Fe_3O_4 particles would be improved by US irradiation, as reported by Muruganandham et al. [25]. A coarser surface morphology of the reacted Fe_3O_4 particles from the UV/Fe_3O_4/Ox system was observed (Fig. 3c), suggesting the formation of some anonymous iron oxides on its surface. The surface of the reacted Fe_3O_4 particles enduring 1 h of UV/Fe_3O_4/H_2O_2 treatment showed obvious aggregation and the particles surfaces appeared to be covered by iron (hydro)oxides (Fig. 3d) [30]. It indicated that the loss of reactive Fe_3O_4 surfaces would inhibit the efficiency of Fenton-like reaction in the system of direct H_2O_2 addition.

3.3. The role of pre-dissolution phase in three different heterogeneous iron oxides–oxalate systems

As discussed in Section 3.1, an initial SMZ degradation lag period appeared in the UV/Fe_3O_4/Ox system without pre-dissolution. In order to assess the role of the Fe_3O_4 pre-dissolution phase in the overall SMZ degradation kinetics, three comparable systems namely UV/Fe_3O_4/Ox, US/UV/Fe_3O_4/Ox and US/UV/α-FeOOH/Ox systems have been investigated for the degradation of SMZ, with or without the iron oxides pre-dissolution phase.

Fig. 4a and b shows the degradation of SMZ in the three systems without or with 30 min of the pre-dissolution, respectively. It can be clearly seen that a gradual decrease in the SMZ concentration was found along with the reaction time in the UV/Fe_3O_4/Ox system with 30 min of pre-dissolution. This trend was similar to those reported in the photochemical iron–oxides oxalate systems [6,12,14,18,31], suggesting that the dissolved iron–oxalate species in the initial reaction phase would be essential for improving the production of ROS and also accelerating the degradation of SMZ. Appearances of the initial SMZ degradation lag period were not found in either US/UV/Fe_3O_4/Ox system or US/UV/α-FeOOH/Ox system without the pre-dissolution, possibly due to US-induced initial rapid dissolution of iron oxides. The discrepancies in the SMZ degradation efficiency of the US-based systems could be attributed to the different dissolution performances with the different iron oxides used.

Fig. 4c and d presents the corresponding oxalic acid degradation in the different systems without and with the pre-dissolution, respectively. The decomposition patterns of oxalic acid in the different systems were consistent with that of the SMZ degradation. There was marginal adsorption of SMZ and oxalic acid on the iron oxides surface during the pre-dissolution phase. The proportion of oxalic acid adsorbed on the iron oxides surface was much lower than that in the bulk solution, indicating that the photochemical reactions due to dissolved iron–oxalate complexes would dominate the overall radical reactions in the systems.

Fig. 4e and f shows the simultaneous evolution of dissolved iron species during the reaction in the different systems. In the systems without the pre-dissolution, an initial rapid increase followed by a gradual decrease in the concentrations of the dissolved Fe(II) and Fe(III) species were observed in both US-based systems. In the UV/Fe_3O_4/Ox system, concentration of the dissolved iron species followed a trend of a slow release until a plateau was reached. As a result, the initial SMZ degradation lag period in the UV/Fe_3O_4/Ox system could be mainly attributed to the initial slow dissolution of the Fe_3O_4 particles. This relationship could be further evidenced by the results obtained in the corresponding systems with the pre-dissolution. As shown in Fig. 4f, 120 and 170 mmol L^{-1} of dissolved Fe(II) and Fe(III) species were released, respectively, after the pre-dissolution phase, leading to a gradual SMZ degradation pattern without appearance of the initial degradation lag period (Fig. 4b).

In the systems adopting either Fe_3O_4 or α-FeOOH particles, coexistence of dissolved Fe(II) and Fe(III) species was observed. Depending upon the solution pH and concentration of oxalic acid, the dissolved iron–oxalate complexes would be mainly $[Fe^{III}(C_2O_4)_2]^-$, $[Fe^{III}(C_2O_4)_3]^{3-}$, and $[Fe^{II}(C_2O_4)_2]^{2-}$ [14]. $[Fe^{III}(C_2O_4)_2]^-$ and $[Fe^{III}(C_2O_4)_3]^{3-}$ are more photo-activated, and $[Fe^{II}(C_2O_4)_2]^{2-}$ can catalyze H_2O_2 with high efficiency [14]. Therefore, it could be concluded that that the photochemical reactions induced by the Fe(III)-oxalate complexes and the Fenton reaction induced by the Fe(II)-oxalate complexes would occur simultaneously in the above systems, leading to the rapid oxidative degradation of SMZ and oxalic acid. In addition, decrease in the total amount of dissolved iron species were found in the US-based systems over the extended reaction time (shown in the insets of Fig. 4e and f). It could be attributed to the rapid consumption of oxalic acid (Fig. 4c and d) and the increase of solution pH (data not shown).

Examination of two main ROS produced in the systems as a function of reaction time could be used to further clarify the role of the pre-dissolution phase. As seen in Fig. 4g and h, gradual increases in the •OH accumulation with the elapsed reaction time were observed in all systems. Except the UV/Fe_3O_4/Ox system without the pre-dissolution, linear increase in the •OH accumulation with time were observed in all systems, wherein different •OH accumulation rate constant (k_{accum} (•OH)) values are shown in the Fig. 4g and h. The order of k_{accum} (•OH) values in the different systems correlated well with the order of degradation rates of SMZ and oxalic acid. It indicated that the produced •OH would be the dominant oxidant. The highest •OH accumulation rates were achieved in the US/UV/Fe_3O_4/Ox systems, indicating that Fe_3O_4 would be more efficient than α-FeOOH in the sonophotochemical iron oxides/oxalate systems. Concomitant with the slow release of dissolved iron species in the UV/Fe_3O_4/Ox system without the

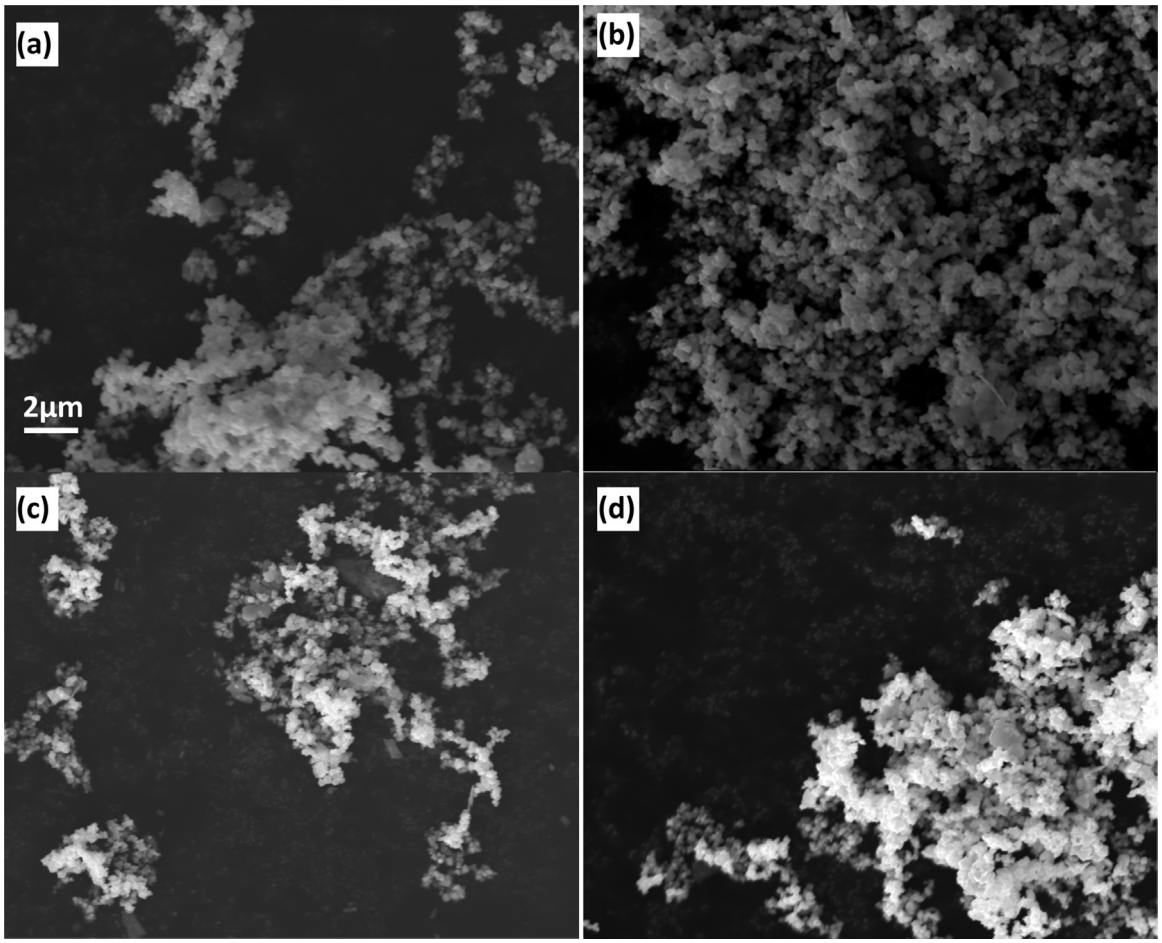

Fig. 3. SEM images of (a) the fresh Fe_3O_4 and the reacted Fe_3O_4 samples after 1 h treatment in (b) the US/UV/Fe_3O_4/Ox system, (c) the UV/Fe_3O_4/Ox system and (d) the UV/Fe_3O_4/H_2O_2 system.

pre-dissolution, a slow production of •OH during the initial reaction period was also observed. This observation could reveal the degradation lag period of SMZ and oxalic acid in the UV/Fe_3O_4/Ox system without the pre-dissolution. In addition, concentration of H_2O_2 was monitored at low level (0–10 μmol L^{-1}) in all systems throughout the whole reaction (shown in the insets in Fig. 4g and h), since the intensive Fenton reaction would occur in the presence of sufficient aqueous Fe(II) species.

3.4. The reaction mechanism in the US/UV/Fe_3O_4/Ox system and promotional role of US

The mechanism of in-situ ROS generation in the homogeneous photochemical iron–oxalate systems has been addressed in the past years [16,32], wherein the photo-reduction of Fe(III)-oxalate complexes ($Fe^{(III)}[(C_2O_4)_n]^{3-2n}$) is the first step triggering a chain of radical reactions for the production of H_2O_2 (Eqs. (1)–(5)). Due to simultaneous generation of ferrous species ($Fe^{(II)}[(C_2O_4)_n]^{3-2n}$) in the presence of oxalic ligand as a result of the reaction shown in Eq. (1), Fenton reaction occurs and leads to the production of •OH (Eq. (6)) as well as the rapid oxidative degradation of target pollutants.

$$Fe^{(III)}[(C_2O_4)_n]^{3-2n} + h\nu \rightarrow Fe^{(II)} + (n-1)C_2O_4{}^{2-} + C_2O_4{}^{\bullet-} \quad (1)$$

$$C_2O_4{}^{\bullet-} + O_2 \rightarrow 2CO_2 + O_2{}^{\bullet-} \quad (2)$$

$$O_2{}^{\bullet-} \leftrightarrow HO_2\bullet(\text{pHdependent}) \quad (3)$$

$$O_2{}^{\bullet-}/HO_2\bullet + H^+ \rightarrow H_2O_2 + O_2 \quad (4)$$

$$O_2{}^{\bullet-}/HO_2\bullet + H^+ + Fe^{2+} \rightarrow H_2O_2 + O_2 + Fe^{3+} \quad (5)$$

$$Fe^{(II)}[(C_2O_4)_n]^{3-2n} + H_2O_2 \rightarrow Fe^{(III)}[(C_2O_4)_n]^{3-2n} + \bullet OH + OH^- \quad (6)$$

The reaction mechanism in the heterogeneous photochemical iron oxides–oxalate systems would be more complicated. Expectedly, there are additional reactions occurring in the solid–liquid interphase which could be the rate-limiting steps to the whole reactions [18]. According to the previous studies [6,14,18,31], the photochemical reactions (Eqs. (1)–(5)) for in-situ H_2O_2 generation and Fenton reaction (Eq. (6)) for •OH production would simultaneously take place on the surface of iron oxides and in the bulk solution. Therefore, the usage of iron oxides with different crystal structures and surface characteristics could lead to remarkable difference in degradation efficiency of the target organic pollutant [18].

Among the solid–liquid interfacial reactions occurred in the photochemical iron oxides–oxalate systems, the dissolution of iron oxides should be the most important rate-governing factor. Cornell and Schwertmann [27] have concluded that there are the three different dissolution mechanisms of iron oxides, i.e., protonation, complexion (in the presence of ligands) and reduction. In the cases of the presence of both oxalic acid ligand and UV irradiation, the dissolution of the iron oxide could be mainly via the complexion and the photochemical reductive dissolution mechanisms, since the protonation dissolution could be negligible with the solid surface adsorption positions occupied by the ligand [33]. The adsorption of oxalic acid ligand on the iron oxide surface could weaken the Fe—O bonds to neighboring atoms and lead to

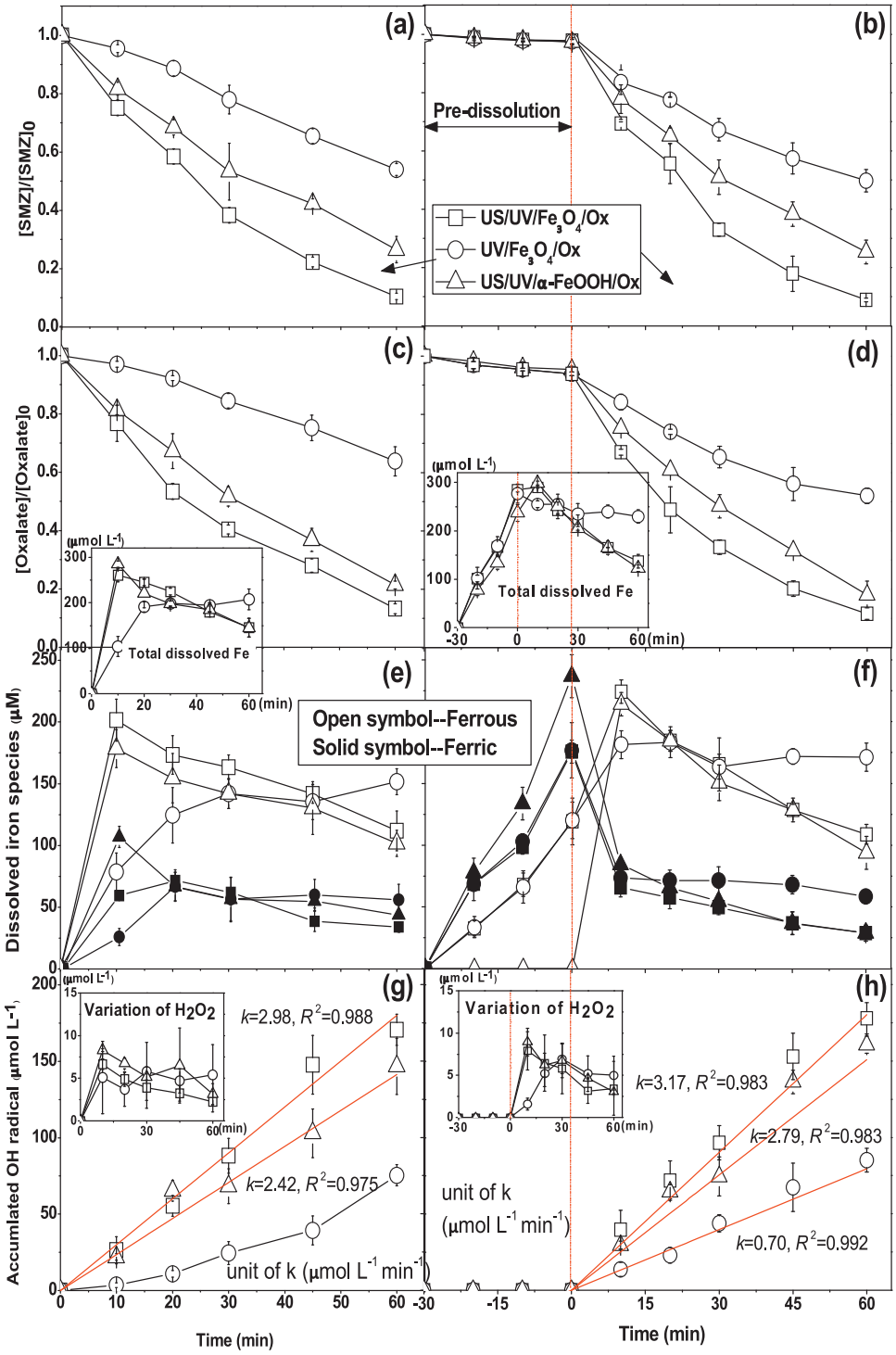

Fig. 4. Evolution of (a) SMZ, (b) oxalic acid, (c) dissolved iron species and (d) reactive oxygen species with elapsed reaction time in the three different systems (left figures: without pre-dissolution, right figures: with 30 min pre-dissolution). Initial parameters: 25 mg L^{-1} SMZ, 0.4 g L^{-1} Fe_3O_4 or goethite, 0.8 mM oxalic acid, 330 W US input power and initial pH 3. Error bars represent 95% confidence limits. Error bars represent 95% confidence limits.

detachment of Fe(III)–oxalate complexes. Meanwhile, the photochemical reductive dissolution could also weaken the structure bonds between Fe atoms in the iron oxides via a photochemical electron transfer (Eq. (1)). It would leading to the reduction of the structural Fe(III)–oxalate complexes in a surface Fe(III)–oxalate complex, followed by the detachment of Fe(II)–oxalate complexes into the bulk solution [27].

On the basis of above analysis, our proposed scheme of reaction mechanism occurring in the UV/Fe_3O_4/Ox system is shown in Fig. 5a, in which an iron cycle with a series of radical reactions are depicted. The complexion dissolution on the Fe_3O_4 surface should occur and initiate the iron cycle. It would lead to the detachment of both Fe(II) and Fe(III) oxalate complexes into the bulk solution, where the preferential detachment of octahedral Fe(III) atom has been generally reported [27]. With a specific inverse spinel crystal structure and the occurrence of Fe(III) in its octahedral and tetrahedral positions, Fe_3O_4 usually dissolves faster than the common natural Fe(III) oxides [33]. The dissolved Fe(II)

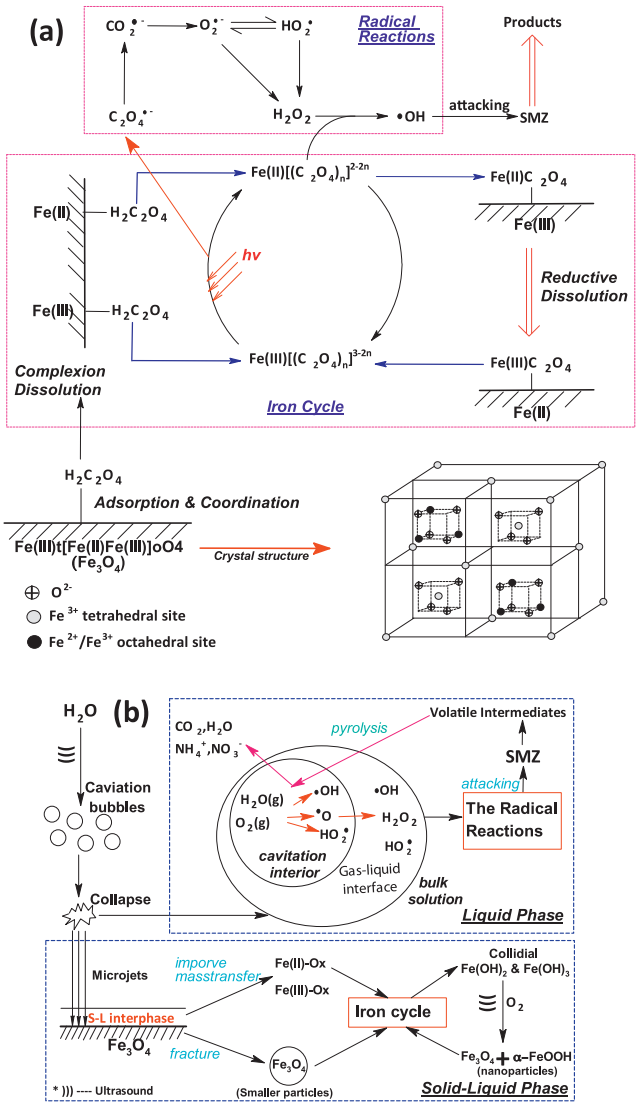

Fig. 5. Schematics of (a) the reaction mechanism in the UV/Fe_3O_4/Ox system, and (b) the promotional role of US in the US/UV/Fe_3O_4/Ox system.

species could further participate in the photochemical reductive dissolution process of Fe_3O_4. Meanwhile, the photo-reduction of Fe(III)$[C_2O_4]_n]^{3-2n}$ in the bulk solution would occur, thus leading to the series of radical reactions (Eqs. (2)–(6)) and the degradation of SMZ.

Furthermore, the promotional role of US in the US/UV/Fe_3O_4/Ox system is also depicted in Fig. 5b. US could induce strong chemical and mechanical effects in the system due to the sonochemical caviation phenomenon [34]. With respect to the heterogeneous US/UV/Fe_3O_4/Ox system, US could have dual promotional effects: (1) promoting the reactions of heterogeneous solid–liquid interphases, and (2) accelerating the homogenous-pahse reactions in the bulk solution.

Under US irradiation, sonochemical thermal dissociation of water and dissolved oxygen molecules in the cavities occurs and leads to the conversion of reactive species such as •OH, •H, and HO_2• in a cavitation bubble [35]. Then a series of radical reactions occur in the gas cavitation bubble, the liquid–bubble interface and the bulk solution, as addressed in the literatures [36,37]. H_2O_2, •OH and HO_2• are the main ROS released to the bulk solution during collapse of the sonochemical bubbles. Apparently, the sonochemical cavitation effect would accelerate the radical reactions in the US/UV/Fe_3O_4/Ox system, leading to more production of •OH and the significant synergistic degradation of SMZ. In addition, as a result of the SMZ decomposition, some volatile organic intermediates/products would be pyrolyzed in the cavitation interior [35,38,39], suggesting an additional mineralization and detoxification of the pollutant.

Besides the above-mentioned US-induced homogenous-phase phenomenon, sonochemical caviation could also induce comprehensive heterogeneous reactions in the solid–liquid interphases (or on the solid surface) (Fig. 5b). As the cavitation bubble collapses, microjets of solvent are formed perpendicular to the solid surface, with an estimated speed of 100 m s^{-1} [34], leading to intensive pitting and erosion of the surface. This phenomenon could also increase the momentum of solid powders in solution, causing the Fe_3O_4 particles fractured upon collision and leading to an overall decrease in the average particle size. Furthermore, the produced shock waves have the potential of creating microscopic turbulence within interfacial films surrounding nearby the solid particles, thus increasing the intrinsic mass-transfer across the film [40]. In summary, the microjets created by US could improve the mass transfer in the solid–liquid interfacial films and lead to decrease of the size of Fe_3O_4 particles (increase of the Fe_3O_4 specific surface area).

It was found that the amount of total dissolved iron species in US/UV/Fe_3O_4/Ox system decreased with the elapse of reaction time (shown in the inset of Fig. 2e), which could be due to the rapid decomposition of oxalic acid ligand and increase in the solution pH. Precipitation of the excessive iron species as iron (hydro)oxides would be expected. US irradiation is an effective method in transforming colloidal $Fe(OH)_3$ and/or $Fe(OH)_2$ into well crystalline iron oxides [41,42], according to the instantaneous supercritical condition (high temperature and pressure) caused by the collapse of cavitation bubbles. In this study, Fe_3O_4 and α-FeOOH would be formed simultaneously under the US irradiation, with respect to the presence of a mixture of F(II) and F(III) precipitants, saturated dissolved oxygen, and weak acidic condition [41]. It could be expected that these two solids would be formed in nanostructure crystals with large surface area, because US generally does not alter the crystalline structure of the primary solids [43], but just alters the transformation of crystal in its presence [44].

3.5. Intermediates, products and the proposed SMZ degradation pathways

In the US/UV/Fe_3O_4/Ox system, organic intermediates of lower molecular weights would be produced along with the simultaneous release of N-containing (organic N) and S-containing (organic S) molecular fragments from the SMZ aromatic rings. These organic N and organic S intermediates could be mineralized, producing inorganic ions. Fig. 6 shows the time-dependent releases of SO_4^{2-}, NH_4^+, NO_2^- and NO_3^- in the US/UV/Fe_3O_4/Ox system, where NO_2^- was not detected throughout the whole reaction. It can be seen in the inset of Fig. 6 that the conversion of organic S to SO_4^{2-} was very efficient, while the conversion of organic N to NH_4^+, NO_2^- and NO_3^- was less efficient. For a SMZ decomposition efficiency of 89.5% (at 1 h of reaction time), 94.5% of organic S containing in the decomposed SMZ molecules were released as SO_4^{2-}. Similar to a previous study [45], this result indicated that the cleavage of S—N bond via •OH attack would be the main SMZ decomposition pathway. In addition, the US/UV/Fe_3O_4/Ox system also achieved a final NO_3^-/NH_4^+ mole ratio of about one order of magnitude larger than that observed in the photocatalytic oxidation of different sulfonamides [45]. It indicated that the sonochemical cavitation effect would accelerate the oxidative transformation of amine intermediates into NO_3^-.

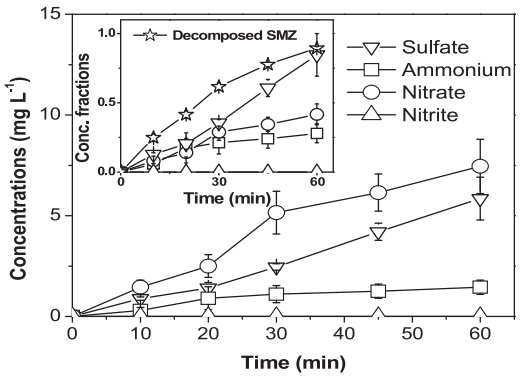

Fig. 6. The evolution of released inorganic ions (SO_4^{2-}, NH_4^+, NO_3^- and NO_2^-) during the SMZ degradation in the US/UV/Fe_3O_4/Ox system. The inset presents the concentration fractions of the released organic S or N correlated to the SMZ decomposition. (Initial parameters: 25 mg L^{-1} SMZ, 0.4 g L^{-1} Fe_3O_4, 0.8 mM oxalic acid, 330 W US input power and pH 3). Error bars represent 95% confidence limits.

Sulfonamides would be transformed similarly under the •OH attack [46,47], and five potential cleavage sites in their molecular structures (Fig. 7) have been proposed by Boreen et al. [48]. In our study, an organic intermediate, 4,6-dimethyl-2-aminopyrimidine, was identified by GC/MS analysis. Based on this result and the degradation pathways reported in the literature [49], we proposed a scheme of the SMZ degradation pathways shown in Fig. 7. A direct cleavage of the δ bond by •OH attack could be one of the main SMZ degradation pathways, followed by the ring-opening of the two intermediates under the continuous •OH oxidation. It would lead to the release of SO_4^{2-} as well as the production of low molecule weight organic amines. Another SMZ degradation pathway, i.e., addition of •OH onto the pyrimidine ring, could be possible too since formation of a hydroxylated intermediate (4-OH-sulfadiazine) as identified by HPLC–MS has been reported in a previous study [49]. The intermediate could be further decomposed with continuous •OH oxidation, leading to the formation of low molecule-weight amines, SO_4^{2-}, NH_4^+ and NO_3^-. In addition, the detection of formate and acetate was also identified by IC (data not shown), indicating further decomposition and mineralization of the amine intermediates.

3.6. Effects of important factors and repeating tests on SMZ degradation

Solution pH affects greatly the reactions occurred in the photochemical Fe(III) oxalate systems, since the speciations of dissolved iron–oxalate complexes is strong pH dependent [16]. With respect to the association forms of oxalic acid at different pH (shown in the inset of Fig. 8a), Fe^{2+} and $[Fe^{II}(C_2O_4)_2]^{2-}$ were concluded as the main ferrous oxalate species at pH < 3 and pH ≥ 3 in the US/UV/Fe_3O_4/Ox system, respectively, while $[Fe^{III}(C_2O_4)_2]^+$, $[Fe^{III}(C_2O_4)_2]^-$ and $[Fe^{III}(C_2O_4)_3]^{2-}$, $Fe(OH_3)_{aq}$ were the main ferric oxalate species corresponding to pH ranges of <2, 2–6 and >6, respectively [14,50]. Fig. 8a presents the variations in pseudo-first-order degradation kinetic constants of SMZ and oxalic acid at different initial pH. It could be concluded that SMZ and oxalic acid have been efficiently degraded in a initial pH range of 2–7, while the best performance was achieved at the initial pH 3–4. This observation agreed with those found in other photochemical or sonophotochemical Fe(III) oxalate systems [16,18,23,51], and was mostly due to the Fe(III) oxalate complexes of higher photoactivity, i.e., $[Fe^{III}(C_2O_4)_2]^-$ and $[Fe^{III}(C_2O_4)_3]^{2-}$ which are dominant at pH 3–4. The more acidic condition (pH 2) inhibited the degradation rates of SMZ and oxalate, possible due to the corresponding ferrous species existing in the form of free Fe^{2+} which proceeds a rate 3–4 orders of magnitude lower than $Fe^{(II)}[C_2O_4]$ in catalyzing H_2O_2 [52]. In addition, increases in the final pHs of the above different systems were also observed as a result of the rapid decomposition of the oxalic acid.

Fig. 8b shows the effect of different dosage ratios between oxalic acid and Fe_3O_4 on the degradation rate constants at a certain initial dosage of 0.4 g L^{-1} Fe_3O_4. The k_{obs} (SMZ) was achieved higher in a dosage ratio range of [Ox]:[Fe_3O_4] (mmol L^{-1}:g L^{-1}) from 1 to 4, while the k_{obs} (Ox) performed a gradual decrease pattern. This is because oxalic acid would play different roles during the reaction in the US/UV/Fe_3O_4/Ox system. In one hand, essential initial concentrations of oxalic acid would form and maintain $[Fe^{III}(C_2O_4)_2]^-$ and $[Fe^{III}(C_2O_4)_3]^{2-}$ as the dominant ferric oxalate species. As reported by Lan et al. [14], a initial 0.8 mM of oxalic acid with respect to 0.4 g L^{-1} of iron oxides would be much enough to form the more photoactive ferric oxalate species. In the other hand, oxalate would compete with SMZ for the •OH oxidative reaction. Apparently, much higher dosage of initial oxalic acid would inhibit the degradation of SMZ as well as oxalic acid itself.

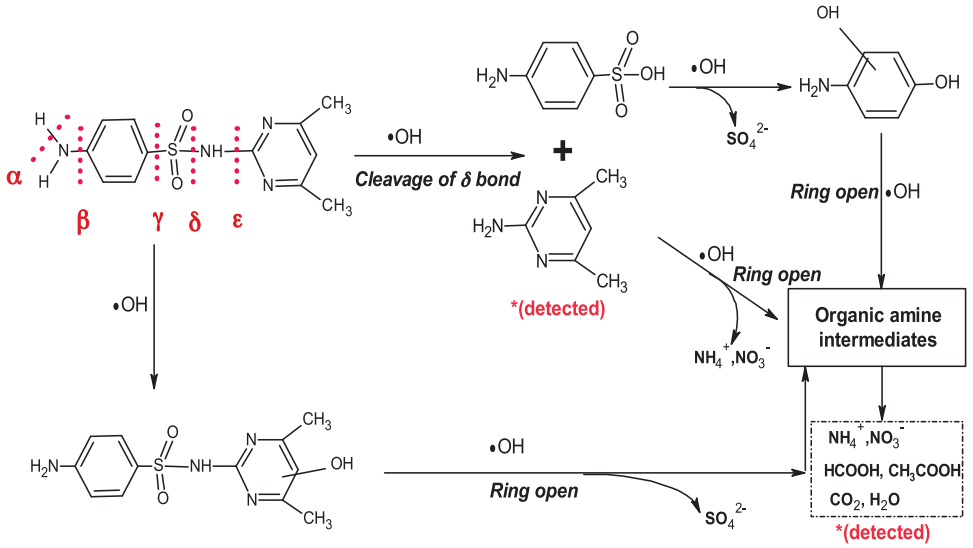

Fig. 7. Proposed SMZ degradation pathways in the US/UV/Fe_3O_4/Ox system.

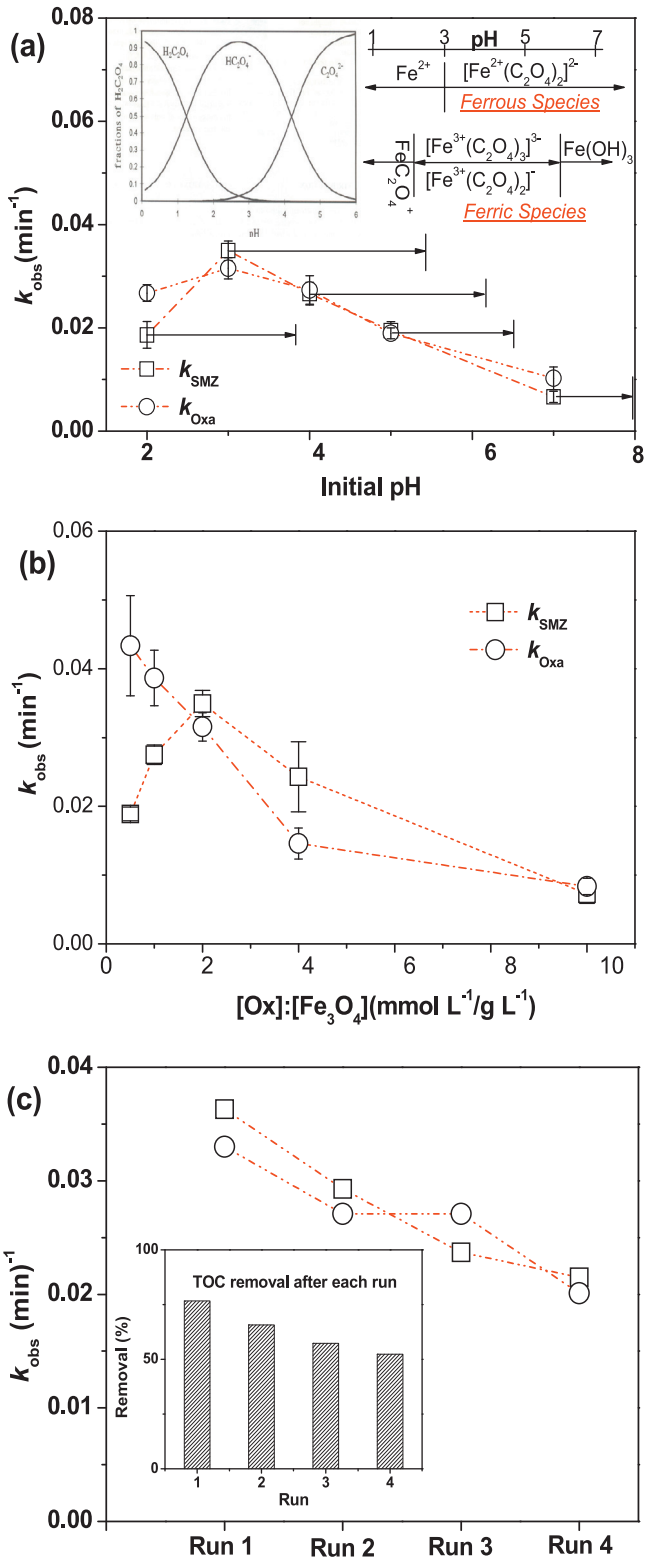

Fig. 8. Effect of (a) initial pH (b) initial molar ratio of [Ox]:[Fe(III)], and (c) repeated runs on the k_{obs} of SMZ and oxalic acid in the US/UV/Fe_3O_4/Ox system. (Except the investigated parameters, the initial parameters were 25 mg L^{-1} SMZ, 0.4 g L^{-1} Fe_3O_4, 0.8 mM oxalic acid, 330 W US input power and initial pH 3). Error bars represent 95% confidence limits).

Repeating test of SMZ degradation in the US/UV/Fe_3O_4/Ox system was also investigated. Four repeating consecutive runs were carried out at the same initial conditions except that the Fe_3O_4 particles were remained magnetically in the reactor before the next run. From Fig. 8c, it was evidenced that fast decompositions of SMZ and oxalic acid could still be achieved in the US/UV/Fe_3O_4/Ox system at the fourth consecutive reaction cycles. This suggested the potential application of the US/UV/Fe_3O_4/Ox system in practical wastewater treatments.

4. Conclusion

In this study, a novel heterogeneous US/UV/Fe_3O_4/Ox system was established for the degradation of SMZ. The US/UV/Fe_3O_4/Ox system could achieve a significant synergistic SMZ degradation, resulting in a significant enhancement in mineralization and detoxification of SMZ. An initial lag period of SMZ degradation appeared in the UV/Fe_3O_4/Ox system without the pre-dissolution phase, while the sonophotochemical iron oxides–oxalate systems could lead to a rapid SMZ degradation even at the initial reaction phase. Examinations of the corresponding evolution of dissolved iron species and ROS produced indicated that the rapid release of dissolved iron species in the initial reaction phases could result in the efficient production of ROS. A scheme of the reaction mechanism in the UV/Fe_3O_4/Ox system is proposed which illustrates simultaneous occurrences of the heterogeneous/homogenous iron cycle and the radical reactions in the homogeneous phase. The promotional role of US in the US/UV/Fe_3O_4/Ox system was concluded, mostly attributable to the sonochemcial cavitation effect in both the heterogeneous solid–liquid interphase reactions and the homogenous bulk radical reactions. Identification of the degradation organic and inorganic products revealed that SMZ degradation was mainly via the pathway involving S—N bond cleavage under the continuous •OH oxidation. Further investigations are recommended to verify the proposed mechanism and to gain further insight into understanding the sonochemical production of iron oxides (Fe_3O_4 and/or α-FeOOH) nanoparticles in the UV/Fe_3O_4/Ox system following the gradual decrease in the total dissolved iron.

Acknowledgments

The authors acknowledge the financial support by Key Project in the National Science & Technology Pillar Program during the Twelfth Five-year Plan Period (No. 2012BAC02B04), Research Fund for the Doctoral Program of Higher Education of China (No. 201201420087), the Fundamental Research Funds for the Central Universities (No. 2014QN144), and SRF for ROCS and SEM. The financial support provided by the National Research Foundation of Singapore through project EWI RFP 0802-11 is also acknowledged.

References

[1] K. Kümmerer, Chemosphere 75 (2009) 417–434.
[2] K.D. Brown, J. Kulis, B. Thomson, T.H. Chapman, D.B. Mawhinney, Sci. Total Environ. 366 (2006) 772–783.
[3] A. Nieto, F. Borrull, R.M. Marcé, E. Pocurull, J. Chromatogr. A 1174 (2007) 125–131.
[4] K. Kümmerer, Chemosphere 75 (2009) 435–441.
[5] M. Klavarioti, D. Mantzavinos, D. Kassinos, Environ. Int. 35 (2009) 402–417.
[6] Q. Lan, F.B. Li, C.X. Sun, C.S. Liu, X.Z. Li, J. Hazard. Mater. 174 (2010) 64–70.
[7] Y. Zuo, J. Hoigné, Environ. Sci. Technol. 26 (1992) 1014–1022.
[8] Y. Zuo, J. Hoigné, Science 260 (1993) 71–73.
[9] M. Vedrenne, R. Vasquez-Medrano, D. Prato-Garcia, B.A. Frontana-Uribe, M. Hernandez-Esparza, J.M. de Andrés, J. Hazard. Mater. 243 (2012) 292–301.
[10] C.Y. Kwan, W. Chu, J. Mol. Catal. A: Chem. 255 (2006) 236–242.
[11] J. Lei, C. Liu, F. Li, X. Li, S. Zhou, T. Liu, M. Gu, Q. Wu, J. Hazard. Mater. 137 (2006) 1016–1024.
[12] C. Liu, F. Li, X. Li, G. Zhang, Y. Kuang, J. Mol. Catal. A: Chem. 252 (2006) 40–48.
[13] Y. Zuo, J. Zhan, Atmos. Environ. 39 (2005) 27–37.
[14] Q. Lan, F.B. Li, C.S. Liu, X.Z. Li, Environ. Sci. Technol. 42 (2008) 7918–7923.
[15] Y. Deng, K. Zhang, H. Chen, T. Wu, M. Krzyaniak, A. Wellons, D. Bolla, K. Douglas, Y. Zuo, Atmos. Environ. 40 (2006) 3665–3676.
[16] J. Jeong, J. Yoon, Water Res. 39 (2005) 2893–2900.
[17] M.E. Balmer, B. Sulzberger, Environ. Sci. Technol. 33 (1999) 2418–2424.
[18] F. Gulshan, S. Yanagida, Y. Kameshima, T. Isobe, A. Nakajima, K. Okada, Water Res. 44 (2010) 2876–2884.

[19] Y. Wu, J. Guo, D. Jiang, P. Zhou, Y. Lan, L. Zhou, Environ. Sci. Pollut. Res. 19 (2012) 2313–2320.
[20] S. Wei, L. Liu, H. Li, J. Shi, Y. Liu, Z. Shao, Appl. Catal., A: Gen. 417–418 (2012) 253–258.
[21] S. Belaidi, T. Sehili, L. Mammeri, K. Djebbar, J. Photochem. Photobiol., A: Chem. 237 (2012) 31–37.
[22] H. Katsumata, T. Okada, S. Kaneco, T. Suzuki, K. Ohta, Ultrason. Sonochem. 17 (2010) 200–206.
[23] T. Zhou, T.T. Lim, X. Wu, Water Res. 45 (2011) 2915–2924.
[24] L.d. Castro, F.P. Capote, Techniques and Instrumentation in Analytical Chemistry, Elsevier, Amsterdam, 2007, pp. 143–192.
[25] M. Muruganandham, J.S. Yang, J.J. Wu, Ind. Eng. Chem. Res. 46 (2007) 691–698.
[26] R. Huang, Z. Fang, X. Yan, W. Cheng, Chem. Eng. J. 197 (2012) 242–249.
[27] R.M. Cornell, U. Schwertmann, The Iron Oxides, WILEY-VCH GmbH & Co. kGaA, Weinheim, 2003, pp. 172–177.
[28] B.M. Voelker, B. Sulzberger, Environ. Sci. Technol. 30 (1996) 1106–1114.
[29] C. Tai, J.F. Peng, J.F. Liu, G.B. Jiang, H. Zou, Anal. Chim. Acta 527 (2004) 73–80.
[30] N. Boonrattanakij, M.C. Lu, J. Anotai, Water Res. 45 (2011) 3255–3262.
[31] F.B. Li, X.Z. Li, X.M. Li, T.X. Liu, J. Dong, J. Colloid Interface Sci. 311 (2007) 481–490.
[32] P. Mazellier, B. Sulzberger, Environ. Sci. Technol. 35 (2001) 3314–3320.
[33] M.A. Blesa, A.D. Weisz, P.J. Morando, J.A. Salfity, G.E. Magaz, A.E. Regazzoni, Coord. Chem. Rev. 196 (2000) 31–63.
[34] K.S. Suslick, Science 247 (1990) 1439–1445.
[35] L.H. Thompson, L.K. Doraiswamy, Ind. Eng. Chem. Res. 38 (1999) 1215–1249.
[36] M. Ashokkumar, J. Lee, S. Kentish, F. Grieser, Ultrason. Sonochem. 14 (2007) 470–475.
[37] H. Yanagida, Ultrason. Sonochem. 15 (2008) 492–496.
[38] A. Kamal, S.F. Adil, M. Arifuddin, Ultrason. Sonochem. 12 (2005) 429–431.
[39] Y.G. Adewuyi, Ind. Eng. Chem. Res. 40 (2001) 4681–4715.
[40] Y.G. Adewuyi, Environ. Sci. Technol. 39 (2005) 8557–8570.
[41] N. Enomoto, J.-I. Akagi, Z.-E. Nakagawa, Ultrason. Sonochem. 3 (1996) S97–S103.
[42] M.D. Luque de Castro, F. Priego-Capote, Ultrason. Sonochem. 14 (2007) 717–724.
[43] L.H. Thompson, L.K. Doraiswamy, Chem. Eng. Sci. 55 (2000) 3085–3090.
[44] R.N. Domingos, D.R. Vollet, A.J. Bucalon, Ultrason. Sonochem. 4 (1997) 321–323.
[45] S. Kaniou, K. Pitarakis, I. Barlagianni, I. Poulios, Chemosphere 60 (2005) 372–380.
[46] P. Calza, C. Medana, M. Pazzi, C. Baiocchi, E. Pelizzetti, Appl. Catal., B: Environ. 53 (2004) 63–69.
[47] S.P. Mezyk, T.J. Neubauer, W.J. Cooper, J.R. Peller, J. Phys. Chem. A 111 (2007) 9019–9024.
[48] A.L. Boreen, W.A. Arnold, K. McNeill, Environ. Sci. Technol. 38 (2004) 3933–3940.
[49] Y. Wang, J.B. Liang, X.D. Liao, L.S. Wang, T.C. Loh, J. Dai, Y.W. Ho, Ind. Eng. Chem. Res. 49 (2010) 3527–3532.
[50] D. Panias, M. Taxiarchou, I. Douni, I. Paspaliaris, A. Kontopoulos, Can. Metall. Q. 35 (1996) 363–373.
[51] Q. Lan, H. Liu, F.B. Li, F. Zeng, C.S. Liu, Chem. Eng. J. 168 (2011) 1209–1216.
[52] D.L. Sedlak, J. Hoigné, Atmos. Environ. A. Gen. Top. 27 (1993) 2173–2185.